12-24-2020

Acid-Triggered Self-Assembled Egg White Protein-Coated Gold Nanoclusters for Selective Fluorescent Detection of Fe^{3+}, $NO2^-$, and Cysteine

Wenyan Li
Shanxi University

Xiangping Wen
Shanxi University

Hemiao Zhao
Shanxi University

Wenjun Yan
Institute of Coal Chemistry Chinese Academy of Sciences

John F. Trant
University of Windsor

Acid-Triggered Self-Assembled Egg White Protein-Coated Gold Nanoclusters for Selective Fluorescent Detection of Fe^{3+}, NO_2^-, and Cysteine

Wenyan Li,[†] Xiangping Wen,[‡] Hemiao Zhao,[†] Wenjun Yan,[§] John F. Trant[*//], Yingqi Li[*†‡]

[†]Department of Chemistry, College of Chemistry and Chemical Engineering, Shanxi University, Taiyuan 030006, P.R. China.

[‡]Key Laboratory of Chemical Biology and Molecular Engineering of Ministry of Education, Institute of Molecular Science, Shanxi University, Taiyuan 030006, P.R.

[§]Institute of Coal Chemistry, Chinese Academy of Sciences, Taiyuan 030001, P. R. China.

[//]Department of Chemistry and Biochemistry, University of Windsor, 401 Sunset Ave., Windsor, ON, N9B 3P4, Canada.

ABSTRACT: Herein, we present a simple and economical synthesis for the first multi-analyte probe able to selectively quantify the concentrations of Fe^{3+}, NO_2^- and Cysteine. It comprises H^+-triggered self-assembled gold nanoclusters (AuNCs@EW/H^+, AuEH) showing enhanced red fluorescence at 640 nm. The AuEH is a good fluorescent nanosensor for Fe^{3+} and NO_2^- with detection limits of 1.40 nM and 2.82 nM, respectively. Iron detection, through fluorescence quenching, occurs due to nanocluster aggregation elicited by the complexation of Fe^{3+} with amino acids on the surface of AuEH; nitrite detection likely proceeds through fluorescence quenching via disassembly of the nanoclusters following irreversible oxidation by nitrite. This selectivity is good enough that it can be used to quantify the nitrite concentration in commercially available processed meat. Cysteine detection occurs through the restoration of fluorescence of iron-quenched samples; similar molecules including homocysteine and glutathione are unable to restore fluorescence showing the specificity of the interaction. Applications, including as a detecting ink and as a biocompatible probe show promise due to the lack of observable toxicity of the AuEH, demonstrating their promise as specific and sensitive biosensors.

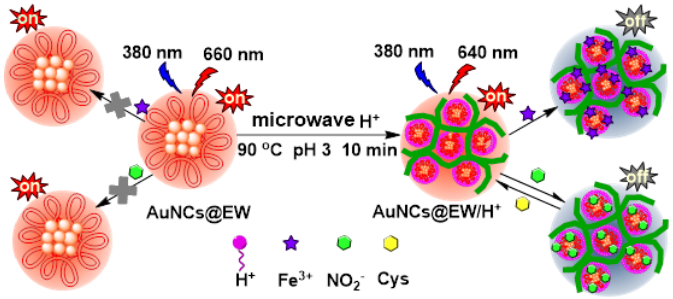

KEYWORDS: *self-assembled, gold nanoclusters, multi-analyte, fluorescent nanosensor, biocompatible probe.*

INTRODUCTION

Nitrites, iron, and cysteine are three very different biologically relevant biomolecules and atoms, each essential, and each toxic at too high a dose.

Nitrite salts, useful for a variety of applications, including as common food preservatives and corrosion inhibitors, have been widely used in drinking water, food and environmental systems, but are both an environmental pollutant and a risk to human health.[1,2] Elevated physiological levels of nitrite both accelerate the irreversible oxidation of hemoglobin (Hb) into high-iron Hb leading to lower oxygen-carrying capacity and hypoxemia,[3] and also react with amines to form carcinogenic nitrosamines.[4]

Iron, generally as Fe^{3+}, likewise plays an important role in many physiological and pathological processes including cell metabolism, enzyme catalysis, and oxygen transport. Insuffi-cient Fe^{3+} again contributes to chronic hypoxemia, leading to hypotension, decreased immunity and anemia. Again, dose matters: excessive levels of Fe^{3+} generates harmful excess reactive oxygen species, leading to damage to nucleic acids, proteins and lipids.[5]

Finally, cysteine (Cys) also has a narrow range of healthy concentrations. Cys deficiency can cause hair discoloration, skin damage, edema, lethargy, liver damage, muscle and fat loss, while ele-

vated levels of Cys can lead to cardiovascular and Alzheimer's disease.[6,7] Cysteine detection is complicated by its functional similarity to homcysteine (Hcy) and reduced

glutathione (GSH). Recently, we reported a GSH-specific detector employing transferrin-protected gold nanoclusters and used this tool to differentiate between cancerous and healthy cells by their endogenous GSH content.[8] We envisioned that a similar technology could provide us with a Cys specific tool.

A variety of diagnostic platforms specific for NO_2^-, Fe^{3+}, and Cys have been developed employing chromatography, fluorescence spectrophotometry, capillary electrophoresis and electrochemical methods.[9-11] However, all face limitations, such as the use of toxic reagents, complex instrumentation, cumbersome and time-consuming sample preparation, and costly/limited selectivity based on the complexity of the ma-trix of the sample.[12-14] Fluorescent gold nanocluster (AuNCs) probes may prove complementary as they offer simple opera-tion, rapid analysis, high sensitivity, and low cost of operation. Most importantly, they offer multi-analyte detection capability: we can use the same AuNC to selectively detect nitrite, iron, or cysteine in a sample. The standard approach to generate AuNCs involves reducing Au^{3+} salts to Au^0 in the presence of molecular templates.[15,16] Guided by the template, gold atoms gradually aggregate to form AuNCs.[17] The size of these clusters, and consequently their emission wavelength, can be controlled by the choice and stoichiometry of reducing agent and capping ligand.[18,19] However, this route provides access to only rather simple AuNCs. Complexity and functionality can be introduced by modifying the surface of the AuNCs,[20-22] but function is still restricted; to the best of our knowledge, employing the same AuNCs for the selective detection of multiple classes of analytes has not been reported.

Herein, we have employed our previously disclosed egg white-functionalized gold nanoclusters (AuNCs@EW, AuE)[23] as the base material to prepare H^+-triggered self-assembled gold nanoclusters (AuNCs@EW/H^+, AuEH) with strong red fluorescence. Egg whites are an extremely inexpensive, avail-able, and easy to use source of protein and if selectivity can be achieved, are far preferable to using expensive isolated pro-teins. These AuEHs specifically recognize Fe^{3+}, NO_2^- and Cys through three different mechanisms. AuEH can detect NO_2^- in food and contributes to the prevention of NO_2^- related diseases. Besides, the study found that the quenched AuEH-Fe^{3+} fluorescence can be restored by Cys alone rather than Hcy or GSH. Scheme 1 shows the preparation of AuEH and the detection of Fe^{3+}, NO_2^- and Cys.

EXPERIMENTAL SECTION

Chemicals and Reagents. Hydrogen tetrachloroaurate trihydrate ($HAuCl_4 \cdot 4H_2O$) was purchased from Zhanyun Chemical Co., Ltd (Shanghai, China). Eggs, Ham sausage (1), Ham sausage (2), Ham sausage (3), Ham sausage (4) and Ham sausage (5) were all purchased from Taiyuan market (Shanghai, China). Stock solutions (0.1 M) of all the cations (Mg^{2+}, Pb^{2+}, K^+, Ni^{2+}, Cd^{2+}, Cr^{3+}, Mn^{2+}, Bi^{3+}, Zn^{2+}, Ba^{2+}, Na^+, Al^{3+}, Co^{2+}, Fe^{3+}, Ca^{2+}, Ag^+, Cu^{2+}, Hg^{2+}) and anions (I^-, Cl^-, SO_4^{2-}, Br-, $S_2O_3^{2-}$, Ac^-, NO_3^-, CO_3^{2-}, NO_2^-, $C_2O_4^{2-}$, F^-, SO_3^{2-}) were prepared by directly dissolving the chloride salts and the sodium salts respectively in doubly-distilled water. Aqueous solutions of disodium-EDTA (EDTA), Cysteine (Cys), Glutathione (GSH), Homocysteine (Hcy), Tyrosine (Tyr), Lysine (Lys), Arginine (Arg), Phenylalanine (PHE), Glucose (Glu), Folic acid (FA), and Ascorbic Acid (AA) were prepared by direct dissolution in ultrapure water purified by a Milli-Q system (Millipore, Bedford, MA) with a resistivity of 18.2 MΩ cm^{-1}. All these standards were purchased from SolibaoTechnology Co., Ltd. (Beijing, China).

Instrumentation. The AuEH was prepared in a Discover SP microwave synthesizer (CEM, Matthews NC, USA). The fluorescence measurements were obtained on a model F-280 spectrophotometer (Tianjin, PRC). The UV-vis absorption spectra were carried out using a Cary 50 Bio UV-vis Spectro-photometer (Agilent, Santa Clara, CA, USA). FTIR spectra of the AuEH were recorded on a FTIR-8400S (Shimadzu Corpo-ration, Kyoto, Japan). The dynamic light scattering (DLS) data were acquired using Malvern Zeta size Nano (Malvern, Malvern, UK) to determine the hydrodynamic diameter and zeta potential of the AuEH. Transmission electron microscopy (TEM) images were obtained using a JEM-2100 TEM (JEOL Ltd, Tokyo, Japan) at an accelerating voltage of 200 kV. The X-ray photoelectron spectrum (XPS) tests were performed on an AXIS ULTRA DLD electron spectrometer (Shimadzu, Kyoto, Japan)

Preparation of AuEH. Gold nanoclusters (AuE) were prepared according to our previous methods.[23] Aliquots (1 mL) were withdrawn, their pH adjusted to 3 using concentrated HCl, and they were transferred into a sealable microwave vessel. The microwave parameters were set to maintain 90 °C for 10 min with intermittent pulsing, and the mixture was premixed for 120 seconds with a high agitation rate prior to heating. Following irradiation, the reaction mixture was centrifuged and decanted, to provide the supernatant as a pale yellow AuEH(HCl) solution exhibiting strong red fluorescence. The differentially activated AuEH(HOAc) and AuEH(H_2SO_4) were synthesized by adding HOAc or H_2SO_4 to the AuE respectively in place of the HCl, using the same method employed for AuEH(HCl). The AuEH solutions were stored at 4 °C until required. No precipitation was observed over several months, and the fluorescent spectra of the stock solutions also remained constant over this period demonstrating the good stability of the nanoclusters.

Selectivity measurement. The AuEH solutions were diluted 10-fold with 0.01M HEPES pH 7.4 buffer (resulting in a final pH of 3.3). Adding 10 μL of 0.1 M solutions of various metal cations (Mg^{2+}, Pb^{2+}, K^+, Ni^{2+}, Cd^{2+}, Cr^{3+}, Mn^{2+}, Bi^{3+},

Scheme 1. Synthesis of the AuEH and a profile of its sensing behaviour towards to Fe^{3+}, NO_2^- and Cys.

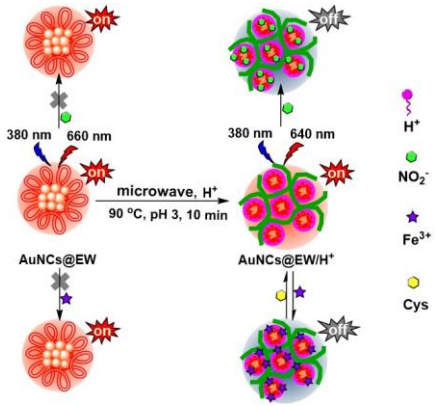

Zn^{2+}, Fe^{3+}, Ba^{2+}, Na^{+}, Al^{3+}, Co^{2+}, Ca^{2+}, Ag^{+}, Cu^{2+}, Hg^{2+}) and anions (I^{-}, Cl^{-},SO_4^{2-}, Br^{-}, $S_2O_3^{2-}$, Ac^{-}, NO_3^{-}, CO_3^{2-}, NO_2^{-}, $C_2O_4^{2-}$, F^{-}, SO_3^{2-}) to 1 mL of the HEPES diluted AuEH system provided the solutions for the cation and anion selectivity studies respectively.

To further investigate the sensitivity of the AuEH sensors for Fe^{3+} and NO_2^{-}, various concentrations of Fe^{3+} or NO_2^{-} standard solutions were prepared by serial dilution in ultrapure water for fluorescent analysis when added to the diluted AuEH solutions.

To investigate the selectivity of the chemical-dependent fluorescence recovery of the quenched AuEH-Fe^{3+} (AuEH diluted 10-fold with HEPES (pH = 7.4) were added with 0.13 μM Fe^{3+}, a final pH of 3.3) system, 10 μL 0.1 M solutions of various biomolecules including Glu and Ascorbic Acid (AA), Phe, Tyr, Lys, Hcy, Cys and a series of ions (Na^{+}, K^{+}, Ca^{2+}, S^{2-}, I^{-}, $C_2O_4^{2-}$, CN^{-}) were added dropwise to the 1 mL of the AuEH-Fe^{3+} system, and the fluorescence emission spectrum were examined.

To further explore the sensitivity of Cys to AuEH-Fe^{3+}, var-ious concentrations of Cys were prepared for analysis by serial dilution using ultrapure water.

Experiments were conducted in triplicate to demonstrate reproducibility. The AuEH fluorescence-quantification experi-ments were then repeated for Fe^{3+}, NO_2^{-} and Cys under both neutral (pH 7.4) and alkaline (pH 8.2) conditions, using the same conditions as described for the acidic (pH 3.3) measure-ments.

Detection of NO_2^{-} content in food. Five different ham sausage brands were purchased from the Taiyuan market in China. 8 g of each finely chopped ham sausage was added to 8 mL of distilled water and sonicated for 30 min to dissolve any NO_2^{-}. The precipitate was removed by centrifugation and the supernatant was filtered 3 times. The obtained liquid was added dropwise to the AuEH solution (using an aqueous solution as a control), and the fluorescence emission spectrum was recorded with a fluorescence spectrometer.

Response time detection analysis. The excitation wavelength was set to 380 nm and the detector set to measure emission amplitude at 640 nm with a 700 s scan time. The AuEH stock solution was then diluted 10-fold with HEPES buffer (0.01 M, pH 7.4), and 1 mL was transferred to a quartz cuvette, to which was added either 10 μL of 0.1 M Fe^{3+} or 0.1 M NO_2^{-}. This sample was then analyzed. For cysteine detection, the AuEH-Fe^{3+} solution (add 12 μL 0.01 M Fe^{3+} to the AuEH solution diluted with HEPES buffer (0.01 M, pH 7.4)) was spiked with 10 μL of 0.1 M Cys prior to data acquisition.

Encoding and decoding of information. A "name" was written on the filter paper (chemical analysis filter paper or fil-lter membrane made of a mixed cellulose ester) using an ink comprising the AuEH solution and the filter paper (or filter membrane) was immediately placed was irradiated under an ultraviolet lamp (365 nm, 16 W) using the ZF7 UV Analyzer at a distance of 20 cm from the lamp for several seconds. A 0.1 M Fe^{3+} solution was then sprayed onto the filter paper (or filter membrane) and illuminated with the same UV lamp (365 nm, 16 W). Finally, a 0.1 M solution of Cys was sprayed onto the filter paper (or filter membrane) and irradiated with the above mentioned ultraviolet lamp.

RESULTS AND DISCUSSION

Synthesis of AuEH. Our previously reported[23] AuE nanoparticles were treated with acid (HCl or HOAc or H_2SO_4), and H^{+}-induced self-assembled nanoclusters (AuEH) were obtained following microwave-irradiation. The fluorescence dependence on pH was investigated to show that intensity was the highest at pH 3 (Figure 1A) and that the maximum emission wavelength of the samples is largely pH independent in acidic solution. This was likely because precipitation was minimized at pH 3, so the fluorescence of the precipitate was the weakest, maximizing the concentration in solution, and hence the fluorescence (Figure 1B); pH 3 was used for all further studies.

Physical and photochemical behaviour of the AuEH nanoclusters. The AuEH solutions have an optimal excitation wavelength at 380 nm and a deep red optimal emission wavelength at 640 nm (Figure 2A). Fluorescence is maintained in the solid state. AuE is an amorphous powder (Figure 2B.1-2), while the protonated chloride and especially acetate clusters are more crystalline. The acetate crystals are also very brightly fluorescent (Figure 2B.4). In contrast, AuEH(H_2SO_4) is an amorphous network and is far darker than the other two mate-rials. This may potentially be due to a denser protein function-alization on the surface of AuEH(H_2SO_4). These results demo-nstrate the macroscopic changes to the materials.

Compared with our previously reported AuE,[23] the optimal emission peak of AuEH is blue-shifted from 660 nm to 640nm

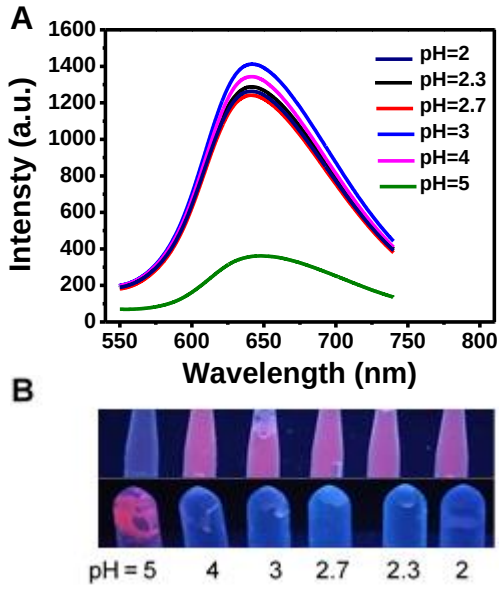

Figure 1. (Effect of pH on the fluorescent profile of AuEH. (A) The fluorescence intensity of AuEH solutions synthesized at different pHs. (B) Photographs of the supernatant (top) and precipitate (bottom) obtained from the AuEH solutions pre-pared at different pHs.

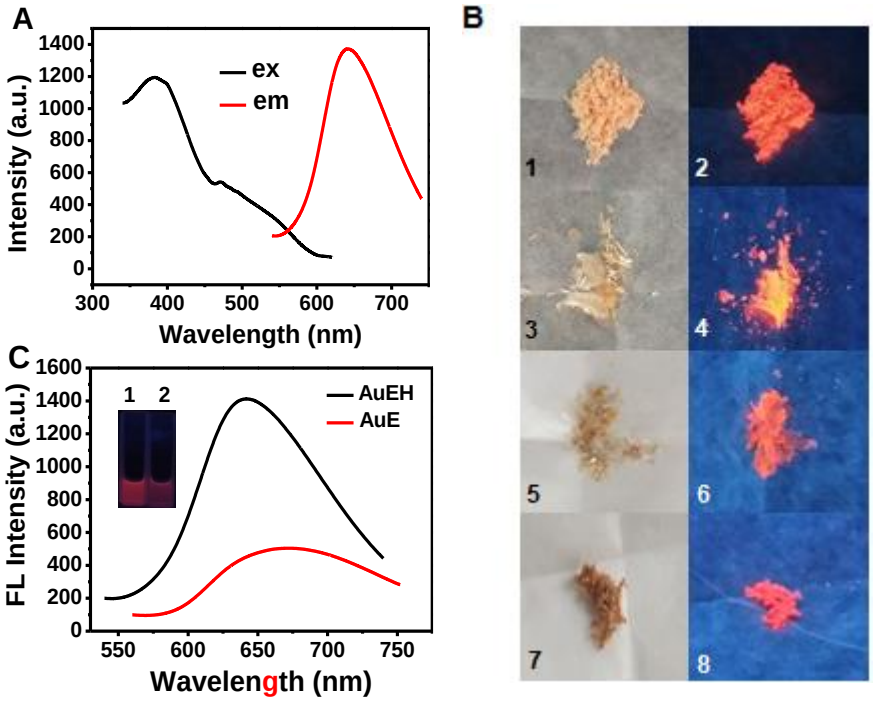

Figure 2. Optical properties of the Au nanoclusters. (A) Fluorescence excitation and emission spectra of AuEH. (B) Photographs of AuE and AuEH, solid powders, under daylight (left panels) and ultraviolet light (right panels) (1-2: AuE; 3-4: AuEH(HOAc); 5-6: AuEH(HCl); 7-8: AuEH(H_2SO_4). (C) Fluorescence emission spectra (excitation slit and emission slits, 5 nm, excitation at 380 nm, concentrations of 0.83 M) of the AuE and AuEH; Inset: photographs of AuEH (1) and AuE (2) under visible (top) and UV light (bottom).

and and fluorescence intensity is enhanced 3-fold (Figure 2C). This is not a factor of pH: when the AuE is adjusted to pH 3, the intensity does not change (Figure S1). The enhanced bright red fluorescence of AuEH aqueous solutions may be ascribed to the fact that the addition of H^+ leads to the inter-complex aurophilic interactions, causing further greater aggregation of the nanoclusters and enhancing fluorescence intensity.[16,24]

To address this hypothesis, TEM was used to determine the morphologies of the acidic nanoparticles, AuEH(HCl) (Figure S2). The particle size of AuEH (3.58 ± 0.72 nm) is significant-ly larger

than that of AuE (1.26 ± 0.415 nm), which is likely a result of acid-induced aggregation due to electrostatic interac-tions between the neutralized proteins on the surface forming the larger clusters (AuEH).[24] These larger aggregates then further self-assemble into even larger AuEH clusters (40 ± 5.83 nm, Figure 3A), which may be responsible for the en-hanced aggregation-induced luminescence. Aggregation, by limiting intramolecular rotation and vibration, reduces the options available for excited state non-radiative relaxation, resulting in this enhancement.[16] The surface of the AuEH has a lattice spacing of 0.25 ± 0.016 nm, which is very similar to the {111} crystal plane of face centered cubic (fcc) Au/Ag,[25,26] with a value of 0.23 nm.

To support the ex situ TEM measurements, we analyzed the particle size using DLS. The average hydrodynamic particle size of AuE is 4.2 ± 0.3 nm (Figure S3A) consistent with the TEM measurement, while the average hydrodynamic size of AuEH(HCl) is greatly increased to 326.2 ± 5.4 nm (Figure S3B). Similarly, the particle sizes of AuEH(H_2SO_4) and AuEH(HOAc) were 214.0 ± 6.1 nm and 173.3 ± 4.6 nm, resp-

ectively (Figure S3C and S3D), indicating that AuEH nanoclusters readily aggregate in water and the TEM does not reflect the true size of the nanoaggregates. The H^+-modified nanocluster solution has a small number of particles with an ultra-small particle size distribution (Figure S3), which may be residual single AuEH nanoparticles. Protonation unsurprising-ly inverts the zeta potential of the negative AuE surface to a strongly positive AuEH surface.

To confirm that the effect was due to protonation and not to the presence of the various anions, we reprepared the materials by adding NaCl, NaAc, and Na_2SO_4 to AuE and then conducting the microwave synthesis. The fluorescence intensity of these gold nanoclusters did not meaningfully increase compared to the original AuE (Figure S4). Likewise, the solid powders obtained from these clusters are similar to the parent compound in terms of fluorescence (Figure S5). The changes seen in the AuEH are consequently far more likely due to protonation than due to the introduction of anions.

Based on the brighter colour of the AuEH(HCl) powder, we selected this formulation for further analysis. AuEH exhibits a distinct absorption peak at 280 nm in the UV spectrum (Figure 3D) with a blue shift relative to the parent AuE particles, suggesting that the surface hydrophobicity of AuEH clusters was enhanced. FTIR analysis shows other differences due to the presence of the proton and the counterions (Figure 3E): the vibration at 787 cm^{-1} is enhanced in AuEH due to the vibration of C-Cl. The absorption peaks of AuEH(H_2SO_4) at 617 cm^{-1} and nd 1174 cm^{-1} are enhanced and broadened because the SO_4^{2-} counterions adsorbed onto the surface of the AuE. Simi larly, the presence of CH_3COO^- resulted in a significant incre-

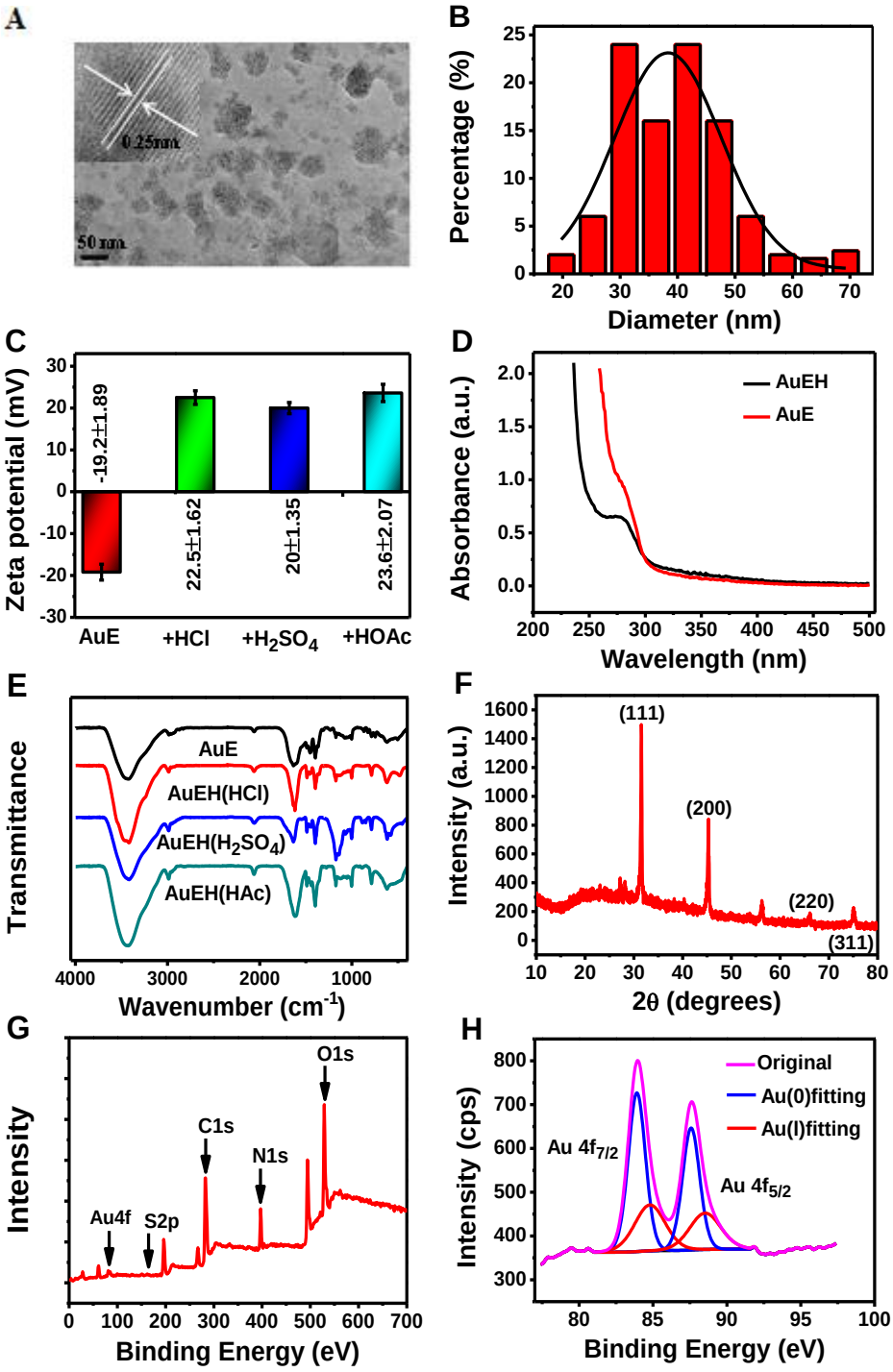

Figure 3. TEM image, and hydrodynamic particle size distribution and zeta potential of AuEH. (A) TEM image of AuEH(HCl), scale bar represents 50 nm. Inset: an expansion showing the lattice spacing of AuEH(HCl) (top); (B) The size distribution histogram and curve of the AuEH(HCl) as determined by TEM of A; (C) Zeta potential of AuE and AuEH(HCl, HOAc, H_2SO_4). Spectral comparison between AuE, AuEH, and the homologues. (D) UV-vis absorption spectrum of both AuE and AuEH; (E) FTIR spectra of AuE, AuEH(HCl), AuEH(HOAc) and AuEH(H_2SO_4); (F) XRD pattern of AuEH. (G) XPS wide survey spectrum of AuEH. (H) Expansion of the XPS spectra of the Au 4f energies portion of the AuEH spectrum in Figure G.

ase in adsorption at both 1640cm^{-1} and the 1398 cm^{-1}, which a--re attributed to the stretching vibration of -C=O and in-plane bending vibration of C-H of methyl group, indicating that the AuEH clusters looks as expected due to more carbonyls. Together, these analyses are likely to support the successful syn thesis of the desired materials.

XRD analysis characterized the crystallite geometry of Au-EH (Figure 3F). The positions of these four diffraction peaks in AuEH are subtly shifted from those of AuE,[23] implying the formation of a new compound. The dominant signals at 31.8° and 45.3° correspond to the (111) and (200) lattice planes as previously observed by others.[27,28] The other two characteristic diffraction peaks at 65.9° and 75.0° correspond to the (220) and (311) lattice planes, respectively. Collectively, the XRD pattern is consistent with our AuEH being a face-centered cubic (fcc) structure.[29]

X-ray photoelectron spectroscopy (XPS) was used to detect the valence and composition of AuEH (Figure 3G, 3H). AuEH is mainly composed of C, N, O, S and Au elements (Table S1). The five peaks at 284.8 eV, 399.9 eV, 531.3 eV, 163.6 eV, 84.0 eV are ascribed to C1s, N1s, O1s, S2p, and Au4f, respectively. This is consistent with what one would expect from egg white protein-coated gold nanoparticles. An expansion of the gold signals clearly shows that the Au4f spectrum is split due to the presence of Au $4f_{5/2}$ and Au $4f_{7/2}$ (Figure 3H). These two bands can be deconvoluted into the Au(0) and Au(I) contributions, with the former clearly dominating.[30] We speculate that an Au(I)-S layer coats an Au(0) core to stabilize the structure of the AuEH analogous to the structures described for sulfhydryl-protected AuNCs.[20,31]

We further studied the stability of AuE and AuEH at different pH conditions as indicated by fluorescence intensity (Figure S6). AuE is stable only under neutral conditions-deviation in either direction changes absorbance; in contrast, AuEH(HCl) is stable between pH 3-12 making it a more useful and versatile sensor as conditions need not be as controlled.

AuEH selectively detects Hg^{2+} and Fe^{3+} through dose-dependent fluorescence quenching. Building on our previous work where we used AuE to identify Hg^{2+} and Cu^{2+},[23] we examined whether AuEH is also suitable for the identification of specific metal ions. We used fluorescence spectroscopy as a screening tool (Figure 4 and S7). The fluorescence of AuEH at 640 nm was quenched by the addition of Hg^{2+} and Fe^{3+} but was unaffected by many other cations. The effect is so pronounced that quantitative fluorescence is unnecessary: a simple visual inspection under 640 nm clearly shows the effect (Figure 4A). This ion selectivity is different from that of Cu^{2+}-selective AuE[23] likely because AuEH agglomerates into larger nanoparticles. Most gold nanoclusters can be fluorescently quenched by Hg^{2+} due to the formation of the very strong Hg^{2+}-Au^{+} interactions on the surface of the nanoclusters.[32,33] The subtle size and elec-trostatic differences between Cu^{2+} and Fe^{3+} are likely responsible for their differing preferences for AuE and AuEH.

The Fe^{3+}-dependent quenching is strongly dose-dependent (Figure 4B, 4C,) with a linear relationship between fluores-cence intensity and Fe^{3+} concentration in the range of 0-6.5 nM, 6.5-99 nM and 0.099-137 μM (Figure 4C inset, 4D, 4E).

This is a very sensitive tool with a detection limit of 1.40 nM from Figure 4C inset (LOD=3σ/S, R^2=0.99, where σ is the standard deviation of the blank measurement, and S and R are the slope and correlation coefficient of the calibration curve, respectively.). These detection limits were compared with previously disclosed methods (Table S2). This analysis indi-cates that, to the best of our knowledge, this system is the most sensitive Fe^{3+}-fluorescent gold nanoparticle sensor reported.

We suspected that the mechanism of Fe^{3+} quenching may involve Fe^{3+} inducing further microscopic aggregation of AuEH. The TEM images of AuEH(HCl) before and after the addition of Fe^{3+} were obtained. Compared with the AuEH nanocluster (Figure 3A), exposure to 13 μM of $FeCl_3$ causes the formation of far larger particles (Figure S8A, 200-500 nm in diameter). This may result from the coordination and cross-linking of the surface protein carboxyl and amino groups by the iron ions as has been previously noted by others.[34,35] Fe^{3+} has been noted to stimulate the aggregation of protein-capped precious metal nanoclusters, which has caused fluorescence to quench.[36,37] This might be the mechanism of action. Like the fluorescent spectrum, the UV-vis spectra of AuEH(HCl) are affected by the addition of Fe^{3+} (Figure S8B). The presence of Fe^{3+} (50 μM) results in a new peak at 310 nm consistent with the absorption peak of free Fe^{3+}; however, as the excitation and emission spectra of AuEH(HCl) do not overlap with the absorption spectra of Fe^{3+} (Figure S8C), no fluorescence resonance energy transfer can occur.[38,39] Further evidence of the surface interaction of the iron with the nanoparticle is provided by the change in the zeta potential of the cluster from + 22.5 mV to + 30.13 mV (Figure S8D). Addition of Fe^{3+} stimulates the further aggregation of AuEH(HCl), which causes fluorescence quenching.

The Hg^{2+} specificity was expected, but the selectivity of the Fe^{3+} detection is very notable. Interference from other ions is a distinct possibility, so we further explored the limits of this Fe^{3+} selectivity. The result is a pleasant surprise. The presence of other metal ions, has almost no effect on the detection of Fe^{3+} by the AuEH system (Figure S9). We were concerned that other redox-active metals such as copper or even Fe^{2+}, can also undergo charge transfer from the reduced to oxidized states and could confuse the measurement; consequently, we also tested Fe^{2+} and Cu^{+}. Fe^{2+} has a negligible effect on AuEH fluorescence (Figure S9A). As copper (I) salts are unstable and poorly soluble in water, we used ascorbic acid (AA) to reduce Cu^{2+} to obtain Cu^{+} *in situ*.[40] Of course, this introduced a contaminant, and we consequently independently determined that AA had no effect on AuEH fluorescence even at high concentrations (Figure S9B). To improve the stability of the copper salts, we also employed EDTA to complex with Cu^{2+}. Therefore, we also quantified the influence of Cu^{2+}•EDTA on the fluorescence of the AuEH; this complex likewise had no measurable effect (Figure S9C). Finally, we used AA to reduce Cu^{2+} into Cu^{+} and tested the effect of Cu^{+} on the fluorescence of the AuEH. In this case Cu^{+} does partially reduce AuEH fluorescence, but the effect is mild (Figure S9C). AuEH has remarkably selective specificity for Fe^{3+}.

The one great confound of course, is mercury. As both Fe^{3+} and Hg^{2+} can quench AuEH fluorescence, the interference of

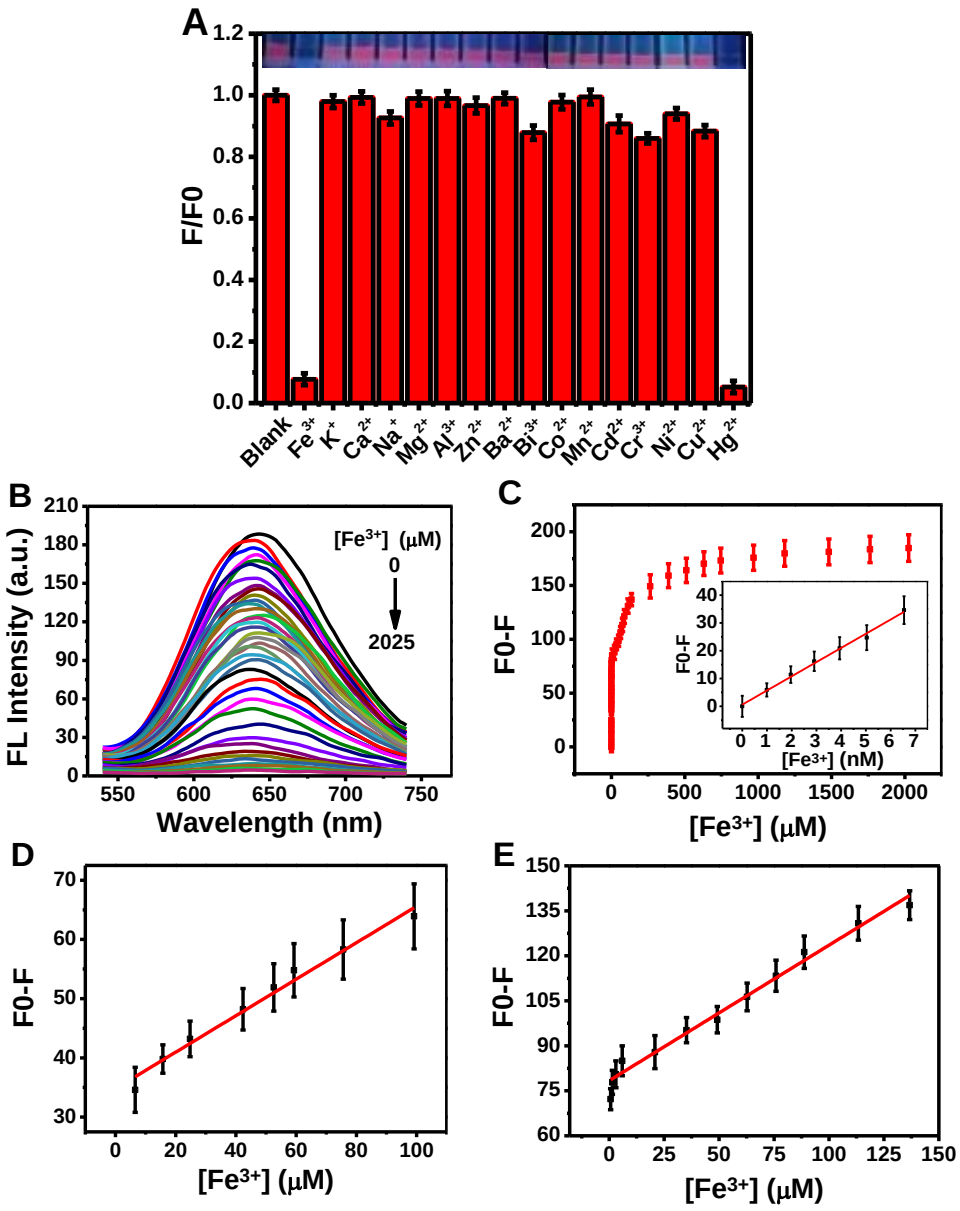

Figure 4. Detection of Fe^{3+}. (A) Effect on AuEH(HCl) fluorescence (F/F0) of different cations (F/F0, where F and F0 are the fluorescence intensities of AuEH(HCl) with and without metal cations (1.0 mM), respectively), inset: photos of the AuEH(HCl) solutions under 640 nm; (B) Fluorescence emission spectrum of different concentrations of Fe^{3+} added to AuEH(HCl). (C) Relative fluorescence intensity (F0-F) of AuEH(HCl) treated with various concentrations of Fe^{3+}. (C inset, D, E) Linear plot of (F-F0) and Fe^{3+} concentration.

Hg^{2+} on the detection of Fe^{3+} must always be considered when quantifying the latter. To be able to address this challenge experimentally, we took advantage of the strong tendency for Hg^{2+} and I^- to form $[HgI_4]^{2-}$.[41] Based on this precedent, we used I^- to remove Hg^{2+} from solution so that iron-mercury mixed systems could be analyzed. Solutions of I^- have little impact on the fluorescence of AuEH (Figure S10). Similarly, when Na_2HgI_4 is added to AuEH, the fluorescence intensity exhibits negligible change (Figure S10). When Fe^{3+} was added to this mixture, quenching occurs. The presence of the mercur- ric iodide does not inhibit iron's interaction with the nanopar-ticle (Figure S10). Iodide can consequently be used as a masking agent for Hg^{2+}, so that the AuEH can be used to quantify Fe^{3+} levels in potentially mercury-contaminated samples.

The sensitivity tests were done in triplicate with fresh synthetic samples (Figure 4, S11). The fit was the same in all cases, and the calculated detection limits were 1.40 nM, 1.43 nM and 1.39 nM (Figure 4C, S11C inset), a relative standard error of 1.5%.

Sensitivity of NO_2^- and fluorescence quenching studies. The presence of adsorbed H^+ on the AuEH led us to speculate that the

addition of specific anions may also quench AuEH fluorescence. Using fluorescence as a screening tool we exam-ined the effect of various sodium salts on AuEH(HCl) optical

behaviour at 640 nm. Only nitrite affected fluorescence (Figure 5A, S12A and S12B). Again, like with iron, the effect is selective and drastic and can be observed from inspection alone (Figure 5A inset). Importantly, unprotonated AuE was not sensitive to NO_2^- (Figure S12C). Again, the effect is dose-dependent (Figure 5B, 5C). When the concentration of NO_2^- is in the range of 0-24 nM and 0.4-64 μM, there is a linear relationship between the relative fluorescence intensity of AuEH and the concentration of NO_2^- (Figure 5D, 5E), and the detection limit calculated from Figure 5D is 2.82 nM (R^2 = 0.99). The detection limit is very low and demonstrates that AuEH can be an excellent probe for detection of NO_2^- with far lower limits of detection than other methods (Table 1). This sensor is also highly reproducible (Figure 5, S13). Triplicate experiments determined detection limits of 2.82 nM, 2.84 nM and 2.86 nM (Figure 5D, S13D) respectively, with a relative standard error value is 0.70%.

As far as we know, there are very few reports using gold nanoclusters to detect NO_2^-.[48] The mechanism of action is certainly not understood. The effect is obviously not a result o-

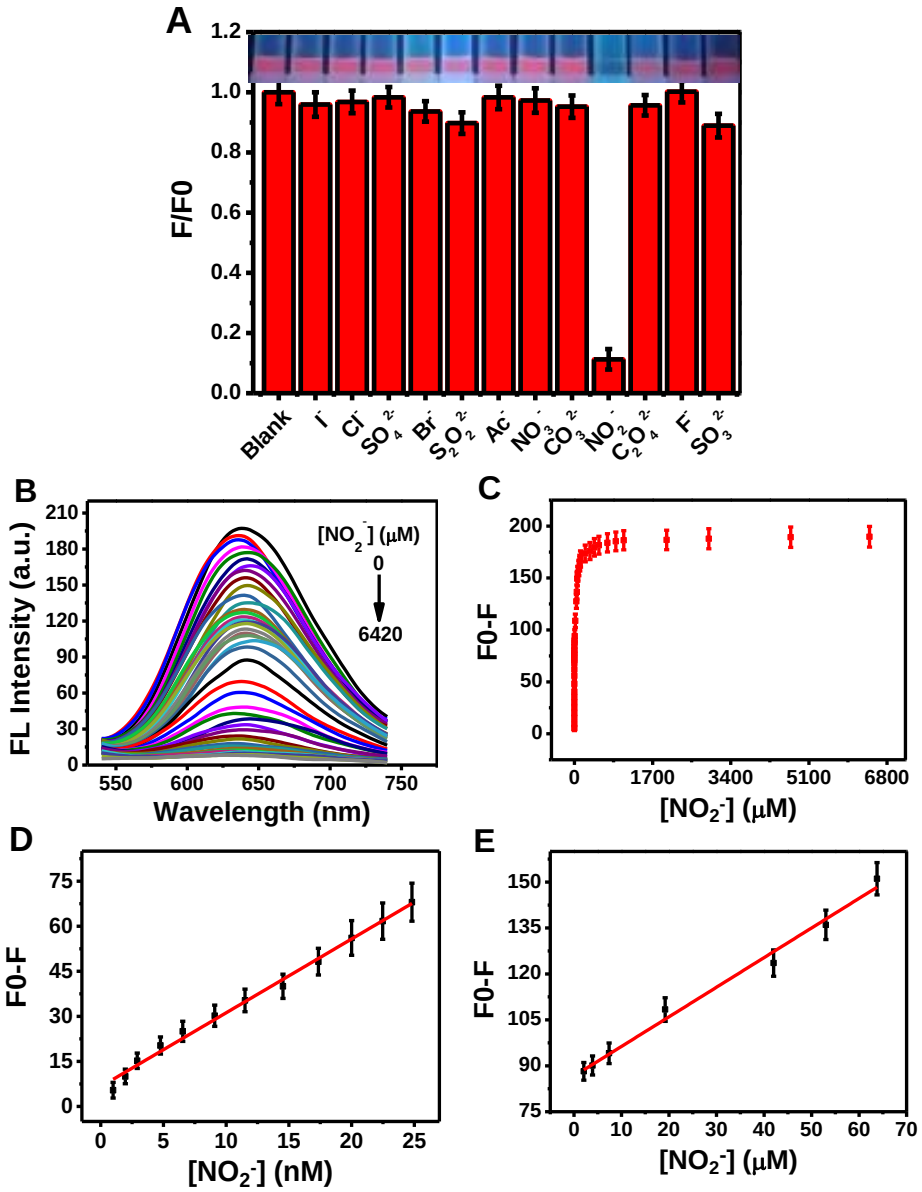

Figure 5. Detection of NO_2^-. (A) Relative fluorescence intensity of AuEH(HCl) (F/F0, where F and F0 are the fluorescence intensities of AuEH(HCl) with and without anions (1.0 mM), respectively), inset: photographs of AuEH(HCl) solutions in the presence of the different metal

ions under 640 nm. (B) Fluorescence emission spectra of AuEH(HCl) as a function of NO_2^- concentration. (C) Relative fluorescence intensity (F0-F) of AuEH(HCl) at 640 nm when treated with various concentrations of NO_2^-. (D-E) Linear plot of (F-F0) and NO_2^- concentration.

Table 1. Comparison with some previously reported of detection for NO_2^-.

Probes	LOD of NO_2^-(nM)	refs.
Rho-MCM@Core and RSho-MCM@Core composite	400	Cui X et al. (2017) (reference 42)
Folic acid probe	18	Lu L et al. (2015) (reference 43)
Au@SiO_2-CdTe@dBSA NPs	60	Liu Y L et al. (2014) (reference 44)
BSA-Au_{25} nanoclusters	100	Unnikrishnan et al. (2014) (reference 45)
Rh 6G-functionlized silica NPs	1200	Wang L L et al. (2012) (reference 46)
(PA) probe	42	Gu B et al. (2016) (reference 47)
AuEH(HCl)	2.83	this work

basicity or simple deprotonation of the nanoclusters as both slightly weaker (acetic, carbonic) and slightly stronger (thio-sulfuric, sulfuric acid monobasic) acids show no activity. It must be due to a more complex interaction. The detector is only functional under acidic conditions, where NO_2^- can coor-dinate with H^+ to form nitrous acid (HNO_2). Upon further protonation, this can reversibly decompose to nitrosyl cations (NO^+) and water.[49] Since NO^+ is an extremely potent oxidant, one can speculate that it may undergo a redox reaction with the Au(I) or Au(0) onto the AuEH, potentially quenching the fluorescence. To validate this mechanism, we examined the morphology and chemical makeup of AuEH(HCl) after addi-tion of nitrite. The morphology of AuEH as determined by TEM does change significantly upon exposure to nitrite (Figure S14): the nanoclusters disassemble with a discernable particle size of 5.5 nm. Moreover, XPS patterns of AuEH(HCl) were also tested after treatment with NO_2^-. XPS analysis demonstrates that the introduction of NO_2^- diminishes the peak intensity of each element (Figure S15A vs Figure 3G). The peak position of binding energy of each element also shifts (Tables S1 and S3), suggesting that the chemical environment of the element has changed. Introducing nitrite decreases the percentage of Au, demonstrating that it decreases the amount of bare gold on the surface. The binding energy (BE) of Au $4f_{7/2}$ electrons, assigned as Au(0), in AuEH is 84.8 eV in the absence of NO_2^-. After adding NO_2^-, BE increased slightly to 85.2 eV (Figure S15B), indicating that the average oxidation state of Au increased. This would be consistent with NO^+ oxidation of surface Au(0) to Au(I). This would possibly destabilize the surface interactions sufficiently to cause disassembly of the nanoclusters which would result in fluorescence quenching. If the interaction were purely physical, a thorough washing process should restore fluorescence due to reversible removal of the nitrate from the surface. However, no matter how the nanoparticles are treated through washing, the fluorescence quenching cannot be reversed, indicating that this process is irreversible. Providing further support, under neutral or alkaline conditions, the introduction of NO_2^- failed to quench the fluorescence of the clusters (Figure S19A). This is good support for the proposed mechanism of action.

Furthermore, that this effect is specific to AuEH rather than AuE was confirmed by treating the sodium salts of AuE with the analytes (Figure S16). Mercuric ions still quench fluores-cence, but Fe^{3+} quenching is far more moderate, and NO_2^- has little effect on fluorescence intensity at all. This is further evi-dence that acid-mediated microwave synthesis is providing a distinct new species.

Detection of NO_2^- content in food. $NaNO_2$ is a common food additive as it is antiseptic without affecting the color, aroma, or taste of food. However, NO_2^- is also carcinogenic, and excessive consumption can cause harm to the body.[50,51] Therefore, NO_2^- content is strictly regulated around the world, although enforcement, as always, remains challenging. These AuEH particles could be very useful tools for regulators. To demonstrate the proof of concept, we purchased five different brands of ham sausages readily available in the Chinese mar-ket and evaluated their NO_2^- content (Table 2). Nitrite content in Chinese processed meat products cannot exceed 30 mg/kg (GB 5009. 33-2010). All five tested below this threshold, but there was still considerable variability, with one sample com-ing very close to the legal limit. This technique took only 1 minute per sample and required none of the complicated in-strumentation or sample preparation normally required for this analysis. Comparing the results with those acquired using the standard spectrophotometric method[52,53] showed that our measurements are within the error range, indicating the validi-ty of the method.

Ham sausage, however, also contains Fe^{3+}, and this could be affecting the measurement; EDTA was added to chelate the iron to remove it from the assay.[54,55] EDTA alone had no effect on the fluorescence of AuEH (Figure S17A). We then investigated the efficacy of employing EDTA as a masking agent for Fe^{3+}. A preformed EDTA•Fe^{3+} complex does still sli-

Table 2. Validation of AuEH(HCl) as an analysis tool to determine NO_2^- content in food.

ghtly decrease the fluorescence of the AuEH solution (Figure S17C); however, when NO_2^- was then added to this EDTA•Fe^{3+}•AuEH mixture, the fluorescence of AuEH was quenched to the same degree as if the nitrate was the only species present (Figure S17C). EDTA can be used as a partial masking agent. Therefore, we can say that the strong binding effect of EDTA and Fe^{3+} allows EDTA to be used as a mask-ing agent so that the detection of NO_2^- by AuEH is not significantly affected by Fe^{3+}. AuEH fluorescence intensity is inversely proportional toNO_2^- concentrations (Figure 5). When the NO_2^- concentration was increased from 0 to 2500 μM, the fluorescence intensity of the AuEH was gradually quenched (Figure S17E). Between 0 and 8.9 nM, the relative fluores-cence intensity of the AuEH is linearly correlated to NO_2^- con centration, allowing us to determine that the detection limit is 1.89 nM, very similar to the limit determine in the absence of EDTA and iron (Figure S17F).

Ham sausage	**Place of origin**	**NO_2^- content by AuEH Analysis(mg/kg)**
(1)	Henan Province	21.4
(2)	Henan Province	22.2
(3)	Jiangsu Province	22.2
(4)	Guangdong Conghua	28.6
(5)	Guangdong Province	11.7

This EDTA-masking protocol was employed to quantify the NO_2^- levels in the ham sausage in order to prevent the interfer-ence of the endogenous Fe^{3+} providing an overestimated result.

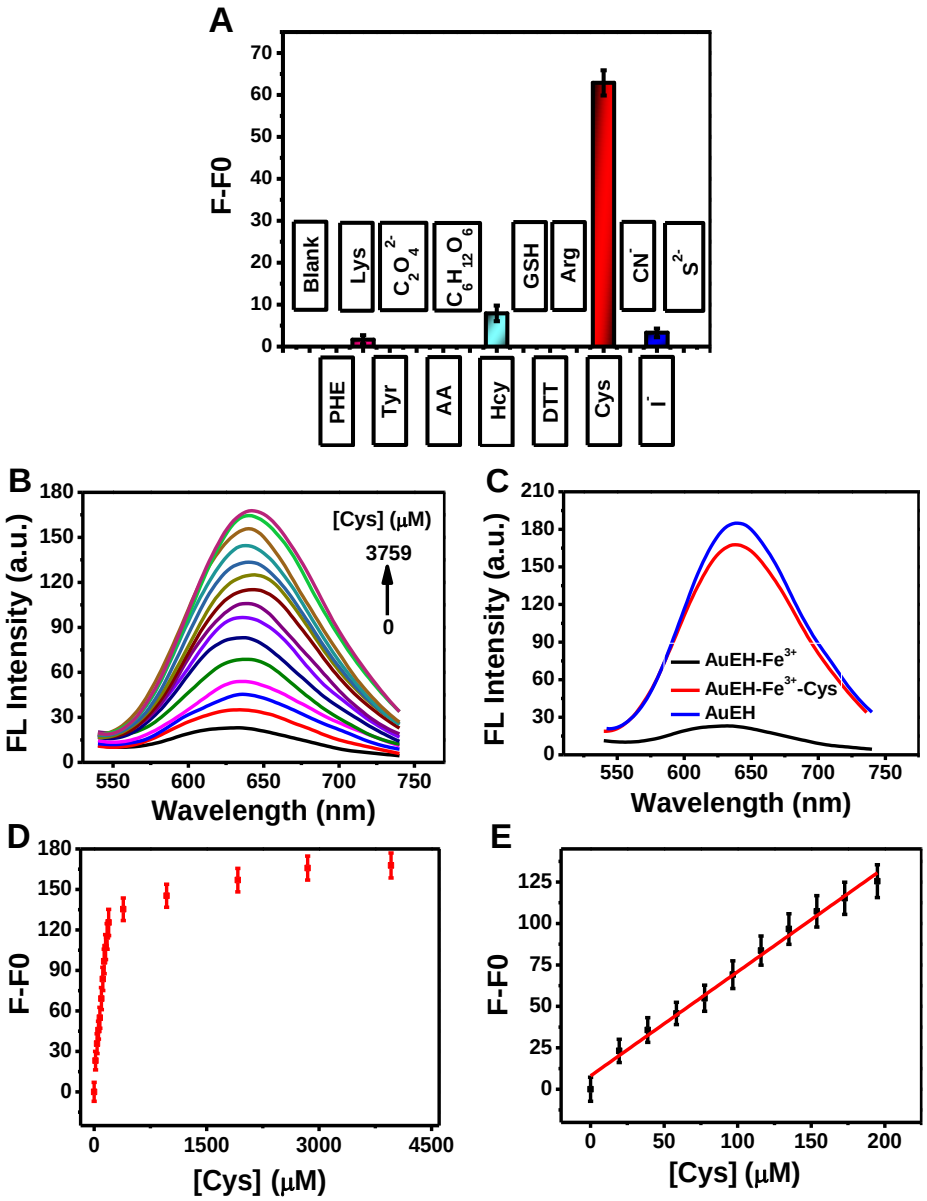

Figure 6. Cysteine-induced fluorescence recovery. (A) The relative fluorescence intensity of the AuEH(HCl) (where F and F0 are the fluorescence intensities of the AuEH(HCl)-Fe^{3+} in the presence or absence of biomolecules, respectively); (B) The AuEH(HCl)-Fe^{3+} fluorescent amplitude dependence on Cys-concentration; (C) The fluorescence intensity of AuEH(HCl), AuEH(HCl)-Fe^{3+} and AuEH(HCl)-Fe^{3+}-Cys (3.8 mM) showing the near complete recovery of fluorescence. (D) Relative fluorescence intensity (F-F0) of quenched AuEH(HCl)-Fe^{3+} treated with different concentrations of Cys. (E) Linear relationship between (F-F0) and concentration of Cys. (B,C,D: Cys concentration from 0-3.8 mM)

By correlating the measured fluorescence obtained from these samples of sausage with our standard curve (Figure S17F), we determined the NO_2^- concentration, and consequently the mass content in the sausage.

Cysteine-induced fluorescence recovery. Abnormal levels of cysteine (Cys) are associated with many human diseases,[56,57] so the detection of Cys remains important. The change in fluorescence intensity of the quenched AuEH(HCl)-Fe^{3+} (AuEH-Fe^{3+}) in the presence of 14 different molecules was determined (Figure 6A). Only Cys effectively restores the quenched AuEH-Fe^{3+} fluorescence. This can be explained by the mechanism that Fe^{3+} can be reduced to Fe^{2+} by Cys, whichis not able to maintain the aggregates, and this leads to fluorescence recovery.[58,59] The effect is dose-dependent (Figure 6B, D) and after reaching 3.8 mM of Cys in solution, 90% of the original AuEH fluorescence is recovered (Figure 6C). The specificity is notable as two other thiol-containing biomolecules, homocysteine and glutathione are incapable of recovering quenched AuEH-Fe^{3+} fluorescence. The cysteine detection limit of the system is 9.87 μM (From Figure 6E) which is not as sensitive as the ion detection capability of the system, but as the normal physiological serum concentration is on the order of 30 μM,[60] this could still prove useful. This detection limit is highly reproducible, with three trials providing values of 9.87 μM, 9.86 μM and 9.89 μM respectively (Figure 6E, S18E), implying a relative standard error of 0.52%.

Evaluation of response time of detection methods. AuEH can detect Fe^{3+}, NO_2^- and Cys with high sensitivity; however the response time is also important. Our time-dependent study indicates that upon addition of Fe^{3+} AuEH fluorescence inten-sity is rapidly quenched, reaching a stable minimum after 341.5 s following *pseudo*-first order kinetics with a rate con-stant of 0.00407 s^{-1} (Figure 7A). The reaction with nitrite, despite being a very different process mechanistically, proceeds in a very similar fashion, plateauing after 353.5 s with a *pseudo*-first order rate constant of 0.00459 s^{-1} (Figure 7B). The efficiency of AuEH fluorescence quenching by Fe^{3+} and NO_2^- is very high; these are not only very sensitive, but are fast responding sensors. The response to cysteine is slower, with the *pseudo*-first-order constant of And for Cys sensing, the results show that the fluorescence intensity of 0.00211 s^{-1} (Figure 7C), however 10 minutes to recovery is still an acceptable length of time for an environmental sensor.

AuEH remains an active sensor under neutral and alka-line conditions for Fe^{3+}, but loses its ability to sense nitrate and cysteine. All of the above studies were conducted in acidic solution; however, the AuEH are still sensitive to Fe^{3+}-induced fluorescence quenching under neutral and alkaline conditions (Figure S19A). However, under neutral or alkaline conditions, NO_2^- becomes unable to affect the fluorescence of AuEH (Figure S19A). This further supports our contention that redox reactions between NO_2^- and the gold surface, under acidic conditions, are responsible for the observed irreversible quenching effect. Similarly, when fluorescent-quenched AuE-

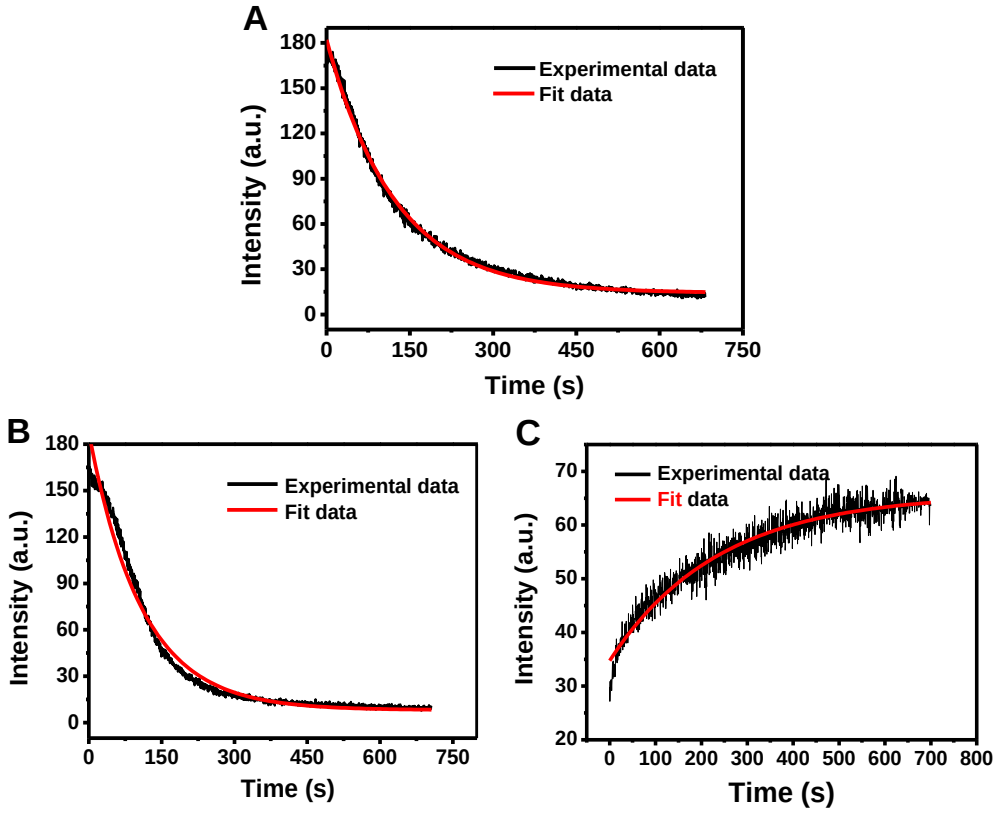

Figure 7. The fluorescence intensity of AuEH(HCl) as a function of time after exposure to ions. (A) Fe^{3+}; (B) NO_2^-; (C) The fluorescence intensity of AuEH(HCl)-Fe^{3+} as a function of time after exposure to Cys.

H-Fe^{3+} is in neutral or alkaline conditions, Cys cannot restore its fluorescence (Figure S19B). This is probably because Cys will not undergo redox reactions with Fe^{3+} above acidic pH. This pH dependence can also be used to ensure that Fe^{3+} can be detected in the presence of NO_2^-: raising the pH makes it insensitive to the anion, while adding EDTA at acidicpH masks the iron. These simple modifications to the sensor conditions means that AuEH can be readily used to detect one analyte in the presence of the other.

AuEH can be used to Encode and decode information and is non-toxic to mammalian cells. This quenching, essen-tially an iron-based off-on switch, could be usefully deployed as an ink. When a word, "AuNCs" was written onto a piece of filter membrane with a solution of AuEH (Figure 8A), it fluo-resces red. When treated with Fe^{3+} the fluorescence is quenched. After adding Cys, the red fluorescence on the filter membrane was restored. Importantly, the AuEH can bind to paper as well, demonstrated by the second example where the Chinese character for "heart" was inscribed on a piece of filter paper (Figure 8B). This use as a fluorescent ink might prove useful as a simple diagnostic tool. This phenomenon may be used to identify the authenticity of consumer products in the future.

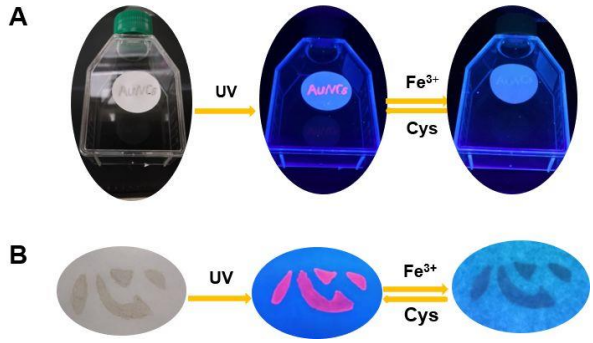

Figure 8. Photographs of AuEH under both visual and UV light (365 nm), alone, or in the presence of iron and/or cysteine. (A) "AuNCs" inscribed on a filter membrane. (B) Chinese character for "heart" inscribed on Whatman filter paper. The second image in the series was acquired from the cysteine restoration of fluorescence.

Additionally, an MTT assay of the AuEH(HCl) against liver HepG2 cells shows no evidence of toxicity up to the maximum tested concentration (1.2 mg/mL; Figure S20A). The nanoclusters exhibit promising cell imaging capabilities as, after incubation, the fluorescence localizes to the cytoplasm (Figure S20B). These could act as in vitro sensors of mercury, iron, elevated cysteine, or nitrite; or, with functionalization, as targetable dyes for other applications.

CONCLUSIONS

In this work, H^+-triggered self-assembled gold nanoclusters (AuEH) were synthesized through the microwave irradiation of egg-white protein-coated gold nanoparticles with HCl. Nanoclusters made with sulfuric acid and acetic acid showed similar activity and properties demonstrating that the effects were due to protonation rather than the specific counterion. The bright red fluorescence of the AuEH can be used to spe-cifically recognize Fe^{3+}, NO_2^- and Cys, and the detection limits are calculated to be 1.40 nM, 2.82 nM, and 9.87 μM, respectively. Fluorescence was largely unaffected by all other analytes except Hg^{2+}. The mechanism of quenching is likely either through the formation of larger aggregates (in the case of Fe^{3+}) or disassembly of the nanoclusters (in the case of nitrite). We used the AuEH to quantify the content of NO_2^- in five kinds of meat products, which indicates that it can be successfully used for quantitative analysis of analytes from real matrices. Inks incorporating AuEH are fast to cellulosic ester membranes and paper under aqueous conditions, and the nanoclusters were deemed non-toxic at all evaluated concentrations. Finally, the use of masking agents, or a simple change in the pH of the solution, makes the AuEH sensitive to only nitrate or Fe^{3+} in real matrices that contain both. They could prove useful as the basis for the development of highly specific biosensors in the future.

ASSOCIATED CONTENT

Supporting Information

The Supporting Information is available free of charge on the ACS Publications website.

A comparison chart of the fluorescence emission, electron microscope, and particle size of AuE and AuEH (Figure S1, S2, S3). Fluorescence emission and histograms verifying that AuEH synthesis is the result of protonation (Figure S4, S5, S16). Plots of cation and anion responses and stability of AuE and AuEH (Figure S7, S12, S6). Table of comparison of Fe^{3+} detected with gold nanoclusters previously reported (Table S2). Figures explaining the mechanism by which iron and nitrite ions quench AuEH fluorescence, respectively (Figure S8, S14, S15). The figures illustrates that AuEH detects Fe^{3+} without interference from other metal ions (Figure S9). A picture describing the detection of Fe^{3+} using AuEH solution after masking Hg^{2+} with I^- (Figure S10). Elemental distribution table of AuEH and AuEH-NO_2^- measured by XPS (Table S1, S3). Figures of repeatability experiment results of AuEH detecting Fe^{3+}, NO_2^- and Cys (Figure S11, S13, S18). Illustration of masking Fe^{3+} with EDTA to eliminate the interference of Fe^{3+} when detecting NO_2^- (Figure S17). Graphs of the fluorescence response of AuEH to Fe^{3+}, NO_2^- and Cys under neutral and alkaline conditions (Figure S19). AuEH biological imaging and cytotoxicity experimental steps and results (Figure S20).

AUTHOR INFORMATION

Corresponding Author

*E-mail: wkyqli@sxu.edu.cn. Tel./Fax: +86-351-7010588.
E-mail: j.trant@uwindsor.ca (J.-F. T)

Notes

The authors declare no competing financial interest.

ACKNOWLEDGMENT

This work is supported by Shanxi Province "1331 project" key innovation team construction plan cultivation team (2018-CT-1), the central government guiding local science and technology development (YDZX20191400002477), Shanxi Science and Technology Development Program (Grant No.201903D321105), and the Canadian Natural Science and Engineering Research Council (NSERC-2018-06338). The authors acknowledge assistance with instrumental analysis from the Scientific Instrument Center of Shanxi University.

REFERENCES

(1) Li, P.; Ding, Y.; Wang, A.; Zhou, L.; Wei, S.; Y, Zhou.; Y,Tang.; Y, Chen.; C, Cai.; T, Lu. Self-assembly of tetrakis (3-trifluoromethylphenoxy) phthalocyaninato cobalt(II) on multiwalled carbon nanotubes and their amperometric sensing application for nitrite. *ACS Applied Materials Interfaces*. **2013**, *5(6)*, 2255-2260.

(2) Rao, H.; Liu, Y.; Zhong, J. Wang, Y. Gold nanoparticle/chitosan@N,S Co-doped multiwalled carbon nanotubes sensor: fabrication, characterization, and electrochemical detection of catechol and nitrite. A*CS Sustainable Chemistry Engineering*. **2017**, *5(11)*, 10926-10939.

(3) Yuan, B.; Zhang, J.; Zhang, R.; Shi, H.; N, Wang.; Li, J.; Ma, F.; Zhang, D. Cu-based metal-organic framework as a novel sensing platform for the enhanced electro-oxidation of nitrite. *Sensors and Actuators B: Chemical*. **2016**, *222*, 632-637.

(4) Li, Y.; Wang, H.; Liu, X.; Guo, L.; Ji, X.; Wang, L.; Tian, D.; Yang, X. Nonenzymatic nitrite sensor based on a titanium dioxide nanoparticles/ionic liquid composite electrode. *Journal of Electroanalytical Chemistry*. **2014**, *719*, 35-40.

(5) Zheng, M.; Tan, H.; Xie, Z.; Zhang, L.; Jing, X.; Sun, Z. Fast response and high sensitivity europium metal organic framework fluorescent probe with chelating terpyridine sites for Fe^{3+}. *ACS Applied Materials Interfaces*. **2013**, *5(3)*, 1078-1083.

(6) Gazit, V.; Ben-Abraham, R.; Coleman, R.; Weizman, A.; Katz, Y. Cysteine-Induced Hypoglycemic Brain Damage: An Alternative Mechanism to Excitotoxicity. *Amino Acids*. **2004**, *26*, 163–168.

(7) Shahrokhian, S. Lead phthalocyanine as a selective carrier for preparation of a cysteine-selective electrode. *Anal Chem.* **2001**, *73(24)*, 5972-5978.

(8) Zhao, H.; Wen, X.; Li, W.; Li, Y.; Yin, C. Copper-mediated On-Off-On gold nanocluster for endogenous GSH sensing to drive cancer cell recognition. *Journal of Materials Chemistry B*. **2019**, *7*, 2169-2176.

(9) Lin, Z.; Dou, X.; Li, H.; Ma, Y.; Lin, J. Nitrite sensing based on the carbon dotsenhanced chemiluminescence from peroxynitrous acid and carbonate. *Talanta*. **2015**, *132*, 457-462.

(10) Ju, C.; Yin, H.; Yuan, C.; Wang, K. A fluorescent probe for both pH and Zn^{2+} based on 2-(1-phenyl-1H-benzo[d]imidazol-2-yl)phenol. *Spectrochimica Acta Part A*. **2011**, *79(5)*, 1876-1880.

(11) Della, B. F.; Vitali, L.; Fett, R.; Costa, A. C. O. Development and validation of a subminute capillary zone electrophoresis method for determination of nitrate and nitrite in baby foods. *Talanta*. **2014**, *122*, 23-29.

(12) Hoch, D. G.; Abegg, D.; Adibekian, A. Cysteine-reactive probes and their use in chemical proteomics. *Chem.Commun*. **2018**, *54*, 4501-4512.

(13) Schierenbeck, T. M.; Smith, M. C. Path to Impact for Autonomous Field Deployable Chemical Sensors: A Case Study of in Situ Nitrite Sensors. *Environ. Sci. Technol*. **2017**, *51*, 4755–4771.

(14) Sahoo, S. K.; Sharma, D.; Bera, R. K.; Crisponi, G.; Callan, J. F. Iron(III) selective molecular and supramolecular fluorescent probes: A Review. *Chem. Soc. Rev*. **2012**, *41*, 7195-7227.

(15) Li, Y.; Zaluzhna, O.; Xu, B.; Gao, Y.; Modest, J. M.; Tong, Y. J. Mechanistic insights into the Brust-Schiffrin two-phase synthesis of organo-chalcogenate-protected metal nanoparticles. *J. Am. Chem. Soc.* **2011**, *133(7)*, 2092-2095.

(16) Luo, Z.; Yuan, X.; Yu, Y.; Zhang, Q.; Leong, D. T.; Lee, J. Y.; Xie, J. From Aggregation-Induced Emission of Au(I)-Thiolate Complexes to Ultrabright Au(0)@Au(I)-Thiolate Core-Shell Nanoclusters. *J. Am. Chem. Soc*. **2012**, *134(40)*, 16662-16670.

(17) Yuan, X.; Luo, Z.; Yu, Y.; Yao, Q.; Xie, J. Luminescent noble metal nanoclusters as an emerging optical probe for sensor development. *Chemistry-An Asian Journal*. **2013**, *44(33)*, 858 – 871.

(18) Lee, D.; Donkers, R. L.; Wang, G.; Harper, A. S.; Murray, R. W. Electrochemistry and Optical Absorbance and Luminescence of Molecule-like Au_{38} Nanoparticles. *J. Am. Chem. Soc*. **2004**, *126*, 6193-6199.

(19) Wu, Z.; Jin, R. On the Ligand's Role in the Fluorescence of Gold Nanoclusters. *Nano Lett*. **2010**, *10*, 2568-2573.

(20) Bai, X.; Xu, S.; Wang, L. Full-range pH stable Au-clusters in nanogel for confinement-enhanced emission and improved sulfide sensing in living cells. *Anal Chem*. **2018**, *90(5)*, 3270-3275.

(21) Li, Z.; Peng, H.; Liu, J.; Tian, Y.; Yang, W.; Yao, J.; Shao, Z.; Chen, X. Plant protein-directed synthesis of luminescent gold nanocluster hybrids for tumor imaging. *ACS Applied Materials Interfaces*. **2018**, *10*, 83-90.

(22) Xu, S.; Nie, Y.; Jiang, L.; Wang, J.; Xu, G.; Wang, W; Luo, X. Polydopamine Nanosphere/gold nanocluster (AuNC)-based nanoplatform for dual color simultaneous detection of multiple tumor-related microRNAs with DNase-I-assisted target recycling amplification. *Anal Chem*. **2018**, *90*, 4039-4045.

(23) Tian, L.; Zhao, W.; Li, L.; Tong, Y.; Peng, G.; Li, Y. Multi-talented applications for cell imaging, tumor cells recognition, patterning, staining and temperature sensing by using eggwhite-encapsulated gold nanoclusters. *Sensors and Actuators B: Chemical*. **2017**, *240*, 114-124.

(24) Qu, F.; L, Zhao.; Han, W.; You, J. Ratiometric detection of Zn^{2+} and Cd^{2+} based on self-assembled nanoarchitectures with dual emissions involving aggregation enhanced emission (AEE) and its application. *Journal of Materials Chemistry B*. **2018**, *6*, 4995-5002.

(25) Chan, Y. H.; Chen, J.; Liu, Q.; Wark, S. E.; Son, D. H.; Batteas, J. D. Ultrasensitive Copper(II) Detection Using Plasmon-Enhanced and Photo-Brightened Luminescence of CdSe Quantum Dots. *Anal. Chem*. **2010**, 82, 3671-3678.

(26) Wang, C.; Yin, H. F.; Chan, R.; Peng, S.; Dai, S.; Sun, S. H. One-Pot Synthesis of Oleylamine Coated AuAg Alloy NPs and Their Catalysis for CO Oxidation. *Chem. Mater*. **2009**, 21, 433-435.

(27) Gui, R.; Jin, H. Aqueous synthesis of human serum albumin-stabilized fluorescent Au/Ag core/shell nanocrystals for highly sensitive and selective sensing of copper(ii). *Analyst*. **2013**, *138(23)*, 7197-7205.

(28) Zheng, B.; Zheng, J.; Yu, T.; Sang, A.; Du, J.; Guo, Y.; Xiao D.; Martin M. F. C. Fast microwave-assisted synthesis of AuAg bimetallic nanoclusters with strong yellow emission and their response to mercury(II) ions. *Sensors and Actuators B: Chemical*. **2015**, *221*, 386-392.

(29) Atchudan, R.; Thomas, N. J.; Edison, I.; Aseer, K, R.; Perumal, S.; Karthik, N.; Lee, Y. R. Highly fluorescent nitrogen-doped carbon dots derived from Phyllanthus acidus utilized as a fluorescent probe for label-free selective detection of Fe^{3+} ions, live cell imaging and fluorescent ink. *Biosensors and Bioelectronics*. **2018**, *99*, 303-311.

(30) Whetten, R. L.; Price, R. C. Nano-golden order. *Science*. **2007**, *318*, 407.

(31) Jadzinsky, P. D.; Calero, G.; Ackerson, C. J.; Bushnell, D. A.; Kornberg, R. D. Structure of a thiol monolayer-protected gold nanoparticle at 1.1 A resolution. *Science*. **2007**, *318*, 430.

(32) Xie, J.; Zheng, Y.; Ying, J. Y. Highly selective and ultrasensitive detection of Hg^{2+} based on fluorescence quenching of Au nanoclusters by Hg^{2+}-Au^{+} interactions. *Chem. Commun*. **2010**, *46*, 961-963.

(33) Xie, J,; Zheng, Y.; Ying, J. Protein-directed synthesis of highly fluorescent gold nanoclusters. *J. Am. Chem. Soc*. 2009, 131, 888-889.

(34) Su, Y.; Qi, L.; Mu, X. Y.; Wang, M. L. A fluorescent probe for sensing ferric ions in bean sprouts based on L-histidine stabilized gold nanoclusters. *Anal. Methods*. **2015**, *7*, 684-689.

(35) Zhao, Q.; Chen, S.; Zhang, L. Y.; Huang, H. W.; Zeng, Y. L.; Liu, F. P. Multiplex sensor for detection of different metal ions based on on-off of fluorescent gold nanoclusters. *Anal. Chim. Acta*. **2014**, *852*, 236-243.

(36) Goswami, N.; Giri, A.; Bootharaju, M. S.; Xavier, P. L.; Pradeep, T.; Pal, S. K. Copper Quantum Clusters in Protein Matrix: Potential Sensor of Pb^{2+} Ion. *Anal. Chem*. **2011**, *83*, 9676-9680.

(37) Ho, J. A.; Chang, H. C.; Su, W. T. DOPA-Mediated Reduction Allows the Facile Synthesis of Fluorescent Gold Nanoclusters for Use as Sensing Probes for Ferric Ions. *Anal. Chem*. **2012**, *84*, 3246-3253.

(38) Qin, L.; He, X.; Chen, L.; Zhang, Y. Turn-on fluorescent sensing of glutathione S-transferase at near-infrared region based on FRET between gold nanoclusters and gold nanorods. *ACS Appl. Mater. Interfaces*. **2015**, *7*, 5965-5971.

(39) Zhao, Q.; Chen, S.; Huang, H.; Zhang, L.; Wang, L.; Liu, F. Colorimetric and ultra-sensitive fluorescence resonance energy transfer determination of H_2O_2 and glucose by multi-functional Au nanoclusters. *Analyst*. **2014**, *139*, 1498-1503.

(40) Song Y. X.; Song Z.; Yang B. S. Spectral study among the Cu^{2+}, ADM and Cop C. *Chem. Res. Chinese Universities*. **2019**, *35(1)*, 53-59.

(41) Kumar, A. M., Jagannath, R., Prithidipa, S., Subhra, K. M., Amarnath, C. Carbazole-thiosemicarbazone-Hg(II) ensemble-based colorimetric and fluorescence turn-on toward iodide in aqueous media and its application in live cell imaging. *Org. Biomol. Chem*. **2012**, *10*, 2231-2236.

(42) Cui, X.; Zhao, Y.; Cui, J.; Zheng, Q.; Wang, B. Synthesis, characterization and nitrite ion sensing performance of reclaimable composite samples through a core-shell structure. Spectrochimica Acta Part A: Molecular and Biomolecular Spectroscopy. 2018, 191, 442-453.

(43) Lu, L.; Chen, C.; Zhao, D.; Yang, F.; Yang, X. A simple and sensitive assay for the determination of nitrite using folic acid as the fluorescent probe. *Anal. Methods*. **2015**, *7*, 1543-1548.

(44) Liu, Y.; Kang, N.; Ke, X. A fluorescent nanoprobe based on metal-enhanced fluorescence combined with FÖrster resonance energy transfer for the trace detection of nitrite ions. *RSC Adv*. **2016**, *6*, 27395-27403.

(45) Unnikrishnan, B.; Wei, S. C.; Chiu, W. J.; Cang, J.; Hsu, P. H.; Huang, C. C. Nitrite ion-induced fluorescence quenching of luminescent BSA-Au_{25} nanoclusters: mechanism and application. *Analyst*. **2014**, *139*, 2221-2228.

(46) Wang L.; Li B.; Zhang L.; Zhang L.; Zhang H. Fabrication and characterization of a fluorescent sensor based on Rh 6G-functionlized silica nanoparticles for nitrite ion detection. Sensors and Actuators B: Chemical. 2012, 171-172, 946-953.

(47) Gu, B.; Huang, L.; Hu, J .; Liu, J.; Su, W.; Duan, X.; Li, H.; Yao, S. Highly selective and sensitive fluorescent probe for the detection of nitrite. *Talanta*. **2016**, *152*, 155-161.

(48) Wu, B. Y.; Wang, C. W.; Chen, P. C.; Chang. H. T. Glutathione assisted preparation of gold nanoclusters using minimum amount of protein. *Sensors and Actuators B: Chemical*. **2017**, *238*, 1258-1265.

(49) Ozawa, S.; Sakamoto, E.; Ichikawa, T.; Watanabe, Y.; Morishima, I. Model studies of nitrosyl intermediates in the catalytic cycle of dissimilatory nitrite reductases. *Inorg. Chem*. **1995**, *34*, 6362-6370.

(50) Walker, R. Nitrates, nitrites and N-nitrosocompounds: a review of the occurrence in food and diet and the toxicological implications: A Review. *Food Addit.Contam*. **1990**, *7*, 717-768.

(51) Kyrtopoulos, S. A. N-Nitroso compound formation in human gastric juice. *Cancer Surv*. **1989**, *8*, 423-442.

(52) Kawakami, T.; Igarashi, S. Highly sensitive spectrophotometric determination of nitrite ion using 5,10,15,20-tetrakis(4-aminophenyl)porphine for application to natural waters. *Analytica Chimica Acta*. **1996**, 333,175-180.

(53) Wu, Q. F.; Liu, P. F. Spectrophotometric determination of micro amounts of nitrite in water and soil. *Talanta*. **1983**, *30(5)*, 374-376.

(54) Xiao, N.; Dong, J. X.; Liu, S. G.; Li, N.; Fan, Y. Z.; Ju, Y. J.; Li, N. B.; Luo, H. Q. Multifunctional fluorescent sensors for independent detection of multiple metal ions based on Ag nanoclusters. *Sensors and Actuators B: Chemical*. **2018**, *264*, 184–192.

(55) Li, C.; Wei, C. DNA-templated silver nanocluster as a label-free fluorescent probe for the highly sensitive and selective detection of mercury ions. *Sensors and Actuators B: Chemical*. **201**, *242*, 563–568.

(56) Seshadri, S.; Beiser, A.; Selhub, J.; Jacques, P. F.; Rosenberg, I. H.; D'Agostino, R. B.; Wilson, P. W. F.; Wolf, P. A. Plasma Homocysteine as a Risk Factor for Dementia and Alzheimer's Disease. *N. Engl. J. Med.* **2002**, *346*, 476–483.

(57) Refsum, H.; Ueland, P. M.; Nygard, O.; Vollset, S. E. Homocysteine and Cardiovascular Disease. *Annu. Rev. Med.* **1998**, *49*, 31-62.

(58) Zhang, L. P.; Ling, B.; Wang, Lun.; Chen, H. Q. A near-infrared luminescent Mn^{2+}-doped $NaYF_4$:Yb,Tm/Fe^{3+} upconversion nanoparticles redox reaction system for the detection of GSH/Cys/AA. *Talanta*. **2017**, *172*, 95-101.

(59) Chen, K.; Qing, W.; Hu, W.; Lu, M. H.; Wang, Y.; Liu, X. H. On-off-on fluorescent carbon dots from waste tea: their properties, antioxidant and selective detection of CrO_4^{2-}, Fe^{3+}, ascorbic acid and L-cysteine in real samples. *Spectrochimica acta. Part A, Molecular and biomolecular spectroscopy*. **2019**, *213*, 228-234.

(60) Brigham, M. P.; Stein, W. H.; Moore, S. The concentrations of cysteine and cystinein human blood plasma. The Journal of Clinical Investigation. 1960, 39 (11), 1633-1638.